Applied Surface Science 681 (2025) 161486

Contents lists available at ScienceDirect

Applied Surface Science

journal homepage: www.elsevier.com/locate/apsusc

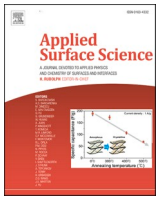

Full Length Article

Influence of the oxidizing technique on the biocompatible and corrosion properties of Ti6Al4V in a physiological environment

Mirjam Bajt Leban [a,*], Tadeja Kosec [a], Aleksandra Kocijan [b], Marjetka Conradi [b], Ita Junkar [c], Janez Kovač [c]

[a] Slovenian National Building and Civil Engineering institute, Dimičeva 12, SI-1000 Ljubljana, Slovenia
[b] Institute of Metals and Technology, Lepi pot 6, SI-1000 Ljubljana, Slovenia
[c] Jožef Stefan Institute, Jamova 39, SI-1000 Ljubljana, Slovenia

ARTICLE INFO

Keywords:
Ti-alloy
Oxide film
Biocompatibility
Surface characterization
Ion release
Simulated body fluid

ABSTRACT

This work aims to evaluate the corrosion and biocompatibility properties of oxide films generated on Ti6Al4V alloys using both traditional and novel methods. Oxide films were generated by anodization and plasma treatment to achieve a blue surface finish. The oxide films were then characterized and compared to a native film formed on the Ti6Al4V.

Electrochemical tests, incorporating potentiodynamic tests and electrochemical impedance spectroscopy, were employed to define the electrochemical resistance of oxides in an environment simulating biological exposure. In vitro tests were conducted to study ion release and biocompatible properties over a 6-week period of exposure to a 0.9 wt% NaCl solution, at body temperature. Various spectroscopic techniques, including ToF-SIMS, XRD, and Raman analysis, were used to study the structure and chemistry of the oxide films. The sub-surface layer was analysed by microstructural investigation.

The type of oxidation was found to have a key influence on the oxide composition, especially with respect to the depth distribution of the individual alloy elements through the oxide film. The oxidation process determines which of the alloying elements are released into the environment, as a result of the corrosion reactions.

1. Introduction

Titanium and its alloys have been successfully used in medicine for decades, fulfilling a variety of applications, including to replace and stabilize bones and for dental implants and vascular stents [1–3]. In addition to their use in the medical sector, components made from titanium and its alloys are indispensable in aerospace as well as many other industries [4,5]. Due to the rapid formation of a passive film when the material comes into contact with any environment that contains even a little oxygen, it exhibits low degradation [6]. This also results in high biocompatibility, which is important for medical applications. The main issues with respect to the biocompatibility of titanium alloys relate to corrosion and surface reactions, interactions with proteins and cells, surface modification and healing in bone [1,2]. Ti6Al4V is a dual phase Ti-alloy consisting of α and β phases. Depending on its thermomechanical history, the microstructure, mechanical properties and also corrosion resistance of the material can vary [7]. Al and V, which respectively act as the α- and β-stabilizers in the microstructure, participate in the composition of a passive film, but their oxides are not as stable as titanium oxide and are released at higher content under contact with a reactive environment [7,8]. The release and accumulation of Al, V, and Ti particles in adjacent tissue could cause health problems, including allergic reactions and carcinogenic or neurological disorders [3,9,10]. Several surface treatments have been studied to reduce the occurrence of such issues, with the aim of optimizing surface topography, roughness and chemical composition. Over the past three decades, at least as much attention has been given to investigating surface treatments for titanium and its alloys as to the optimization of the chemical composition of these materials to achieve the mechanical and corrosion properties desired [11,12]. The most well-known/ studied treatment is electrochemical oxidation, also known as anodization. This process involves the application of different potentials, ranging from ten to several hundred volts, to promote the growth of an oxide film, which can vary in thickness from 10 nm to more than 100 nm, at which depth nanotubes are developed [13–16]. Highly reactive plasma is well-known as an effective surface cleaning agent, the action of which breaks most organic bonds and

* Corresponding author.
E-mail address: mirjam.bajt-leban@zag.si (M. Bajt Leban).

https://doi.org/10.1016/j.apsusc.2024.161486
Received 6 August 2024; Received in revised form 28 September 2024; Accepted 8 October 2024
Available online 10 October 2024

reduces the contact angle (i.e. increases wettability), but it could also be used to oxidize highly reactive metals such as titanium [17–21].

Since the oxide film on titanium alloys represents a barrier between the metal and the environment, it is very important for it to be as stable as possible. Thin titanium dioxide films (TiO_2) can form naturally on the surface of titanium alloys as oxides of a few nm thick (e.g. a passive film), or can be formed artificially by the processes mentioned above and other oxidizing methods [12], leading to oxides ranging in thickness from a few nanometers to several hundred [9]. The crystalline oxide forms most commonly observed on titanium alloys are rutile and anatase, both of which exhibit a tetragonal crystal structure; rarely, other forms (e.g. brookite) are also seen. Rutile (α-TiO_2), which has a denser, more closely-packed structure, is more thermodynamically stable than anatase (β-TiO_2). Anatase can be irreversibly transformed to rutile at temperatures above 600–700 °C, with time and pressure also influencing its transition [22]. Many studies have reported better corrosion behavior when an oxide is in the form of rutile [11,23–25], and it has been shown that the resistance of dual-phase anatase–rutile is improved following thermal oxidation of the anodized surface [26]. The disadvantage of these investigations is that the thickness of the oxides being compared is usually not the same, nor are the substrates identical. Furthermore, the influence of the surface modification technique on the substrate itself, as well as on the microstructure and related differences in the oxides, have been poorly researched and are not well understood. In order to progress one step closer to this knowledge, blue oxide films, which give the surface a blue-like finish, were created on a Ti6Al4V alloy using two different techniques, ensuring the thickness of the oxides remained very similar (approximately 40 nm). When light waves strike a thin oxide on titanium, some of the light is reflected from the uppermost surface of the oxide, while some penetrates the oxide and reflects off the lower surface. The interference effect of the reflected waves results in the creation of interference patterns, which manifest in changes in the perceived color of the titanium surface. The color of the titanium observed depends on the thickness of the oxide [27–29], but is not, however, influenced by the crystalline form of the oxide.

The aim of the present study was to enhance understanding regarding the influence of the oxidation method on the behavior of a Ti6Al4V alloy in a physiological medium. This was achieved through precise characterization of the properties of blue oxides produced by two chemically and physically different methods – namely, electrochemical anodization and plazma oxidation. The properties were compared to those of a native oxide film spontaneously developed on Ti6Al4V. Electrochemical characterization was conducted using potentiodynamic scans and electrochemical impedance spectroscopy during 1 week of immersion. Ion release tests were also performed during 42 days of immersion in a 0.9 % NaCl solution at 37 °C. In-depth microstructural investigation was conducted using Scanning Electron Microscopy (SEM) coupled with Electron Backscatter Diffraction (EBSD). Time-of-Flight Secondary Ion Mass Spectrometry (ToF-SIMS), depth profiling by X-ray photoelectron spectroscopy (XPS), X-ray diffraction (XRD) and Raman analysis were further conducted to study the properties of the oxides.

2. Materials and experimental methods

2.1. Material

A Ti6Al4V alloy was used as the base material, cut from 1.9 mm thick sheets. The chemical composition of the plate used, as determined by optical emission spectroscopy, was 5.85 % Al, 3.92 % V, 0.10 % Fe, 0.01 % Si, and 0.03 % C, with the balance being Ti.

2.2. Oxidation procedures

A reference specimen, denoted in the paper as the “reference”, was first prepared by grinding a piece of the bare (untreated) material with 600 grit SiC paper and cleaning it in acetone for 10 min in an ultrasound bath. This specimen was then placed into a solution consisting of 92 ml distilled water, 6 ml NaOH and 2 ml HF for one minute, then rinsed with distilled water and dried with hot air. The same procedure was then used for all the other specimens before subjecting them to various oxidation treatments, thus coloring their surfaces blue. The specimens oxidized by anodization are denoted as “anodized”. Anodization was carried out in an electrolyte consisting of 20 g/L citric acid and 20 g/L $NaHCO_3$, applying a potential at 30 V for 10 s. The specimens denoted “plasma” were oxidized in a 2-step plasma process, detailed as follows: 1st step – ratio H: O = 6:1, combined pressure: 40 Pa, plasma power: 600 W, time: 42 s; 2nd step − O-plasma, pressure: 30 Pa, time: 30 s.

2.3. Experimental methods

2.3.1. Electrochemical tests

Electrochemical tests were performed in a 0.9 % NaCl aqueous solution at 37 °C. Before electrochemical testing, all samples were rinsed with deionized water and ethanol and air-dried. A jacked three-electrode corrosion cell was used for the electrochemical tests, consisting of a working electrode (a cylindrical flat specimen of diameter 15.0 mm, inserted in the specimen holder, so that an effective area of 0.785 cm^2 was exposed to the solution), a reference electrode (Ag/AgCl/KCl (sat.)), and a graphite rod as a counter electrode. Firstly, open circuit potential (OCP) was measured for 6200 s, then linear polarization measurements (LP) were conducted at a scan rate of 0.1 mV/s in the potential range ± 20 mV vs. OCP. Potentiodynamic (PD) measurements followed, starting from –0.25 mV vs. corrosion potential (E_{cor}), with a potential sweep in the anodic direction up to 3.20 V at a scan rate of 1 mV/s.

Electrochemical impedance spectra (EIS) were measured in the frequency range from 65 kHz to 1 mHz with an AC amplitude of ± 10 mV (peak-to-peak) during 1 week of immersion. EIS measurements were carried out at open-circuit potential (OCP), in a 0.9 % NaCl aqueous solution at 37 °C, at various times of exposure: 0 h, 24 h, 48 h, 72 h, 96 h, 120 h, 144 h, and 168 h. EIS data were fitted using the ZView program (Scribner, Southern Pines, North Carolina, USA). The chi square of fit values was between 0.001 and 0.005.

2.3.2. Ion release test

The ion release (immersion) tests were conducted on square sheets sized 35 x 25 mm. The surface exposed to the electrolyte was limited by a pool constructed by 3D printed walls, with the plastic material glued to the metallic surface and silicon applied at the outer edge between the wall and the metallic surface to prevent the electrolyte leaking through the joint. The pool, which contained 5 cm^2 of the exposed metallic area, was filled with 5 ml of 0,9 % NaCl aqueous solution. The total time of exposure over the course of the immersion test was 42 days. Fresh solution was placed in the pools on the 1st, 4th, 7th, 14th, 21st, 28th, 35th, and 42nd days of the experiment. Three replicates of each of the reference and oxidized specimens were exposed to the testing solution. The concentrations of the Al and V ions in the solution following exposure were measured using an ICP MS Agilent 7900x (Agilent Technologies, Japan). The concentrations obtained were normalized according to the area exposed, such that the results were given as the total amount of ions released per 1 cm^2 of sample exposed. The concentrations of Ti ions released were also measured, but due to the high interference of titanium with the matrix, the relative standard deviation (RSD) was too high to perceive the results as relevant [30].

2.3.3. Time-of-flight secondary ion mass spectrometry (ToF-SIMS) and X-ray photoelectron spectroscopy (XPS)

ToF-SIMS analyses were performed using a ToF–SIMS 5 instrument (ION-TOF, Münster, Germany) equipped with a bismuth liquid metal ion gun with a kinetic energy of 30 keV. The SIMS spectra were measured by scanning a Bi^+ ion beam over an area of 100 × 100 μm^2. SIMS depth

profiles were performed in dual beam depth profiling mode, using the 1 keV Cs^+ ion beam rastering over 0.4 × 0.4 mm for sputtering. In order to verify etching rate, an internal standard – namely an Al_2O_3 oxide layer of known thickness i.e. 30 nm – was sputtered at a sputtering rate of 0.050 nm/s.

The X-ray photoelectron spectroscopy (XPS) analyses were carried out using a PHI-TFA XPS spectrometer (produced by Physical Electronics Inc.) equipped with an Al-monochromatic source emitting photons at an energy of 1486.6 eV. The area analyzed was 0.4 mm in diameter. The surface composition was quantified from the XPS peak intensities, taking into account the relative sensitivity factors provided by the instrument manufacturer [31]. XPS depth profiling was performed by the 3 keV Ar^+ ion beam rastering over an area of 3 × 3 mm, using an etching rate of 1.0 nm/min.

2.3.4. SEM examination of the surface and underlying microstructure

The surface morphology and cross-section of the samples under investigation were evaluated using scanning electron microscopy (FIB-SEM ZEISS Crossbeam 550 SEM). For investigation of the cross sections, metallographical samples were prepared (cross sections of the Ti6Al4V specimens cast in conductive resin), ground, then polished with 0.06 μm colloidal silica.

2.3.5. XRD and Raman spectroscopy

X-ray diffraction (XRD) analysis was carried out using an Empyrean XRD diffractometer (PANalytical, Malvern, UK) and the data analyzed using HighScore Plus database software. The XRD spectra were measured between 4° and 100° (2Θ), using a step size of 0.0065° and a time per step of 61.2 ms.

The Raman spectra of the oxidized samples were recorded by a Horiba Yvon LabRAM HR spectrometer (France, 2009), using a green laser at λ = 532 nm. The scanning range was 50–1000 cm^{-1}, with an accumulation time of 25 s for each acquisition to reach the sufficient number of counts. The background was not subtracted. The oxide film on the reference sample did not give any Raman response and is therefore not presented in the Results section.

3. Results

3.1. Metallographical examination

The microstructures of the specimens investigated are presented in Fig. 1, focusing on the examination area close to the oxidation layer. Cross sections of the oxidized surfaces on the reference (with no artificial oxidation applied), anodized and plasma-treated specimens are presented in Fig. 1 a, b and c, respectively. The microstructure of the reference and anodized specimens consists of equally-distributed equiaxed α-phase (dark grains in the SEM images, marked with white arrows) and discontinuous β-phase at the α-phase grain boundaries (light grey grains, marked with white arrows). In the case of the plasma-treated specimen (Fig. 1c), the microstructure of the cross section near the surface is similar to the microstructural of other two samples, while its bulk microstructure consists of continuous β-phase (marked with a black arrow) in the α-phase grain boundaries. An α + β lamellar microstructure is also observed in the bulk microstructure of the plasma-oxidized specimen.

Metallographic investigation shows that the anodization process has no influence on the microstructure, but a change was observed in the bulk microstructure of the plasma-treated specimen. During plasma treatment, the core of the specimen is inductively heated above the β-transus temperature, at around 980 °C, then cooled at a moderate rate. During this type of treatment, the temperature at the surface remains below the β-transus temperature, probably due to the very short duration of the plasma oxidation process.

3.2. XRD and Raman spectroscopy

XRD spectra reveal the presence of peaks characteristic for the α-phase in all specimens, as shown in Fig. 2. Peaks for the β-phase are not intensive, with their presence only confirmed for the plasma-treated specimen. A significant shift in the peaks toward lower angles was, however, observed in the XRD patterns for the plasma-treated specimen. The shift from 0.2 to 0.6° can be attributed to expansion of the lattice, which is caused by the uptake of oxygen [32]. In addition, the XRD peaks are split in these specimens, with the first peak (at a lower angle) always being lower than the second. A similar splitting of peaks was also observed for all the peaks in the reference specimen, and for the peaks (1 1 0), (103), (112) and (201) in the anodized specimen. Splitting could occur due to cell deformation or distortion [33].

As seen in Fig. 3, Raman bands are visible at 136 cm^{-1}, 394 cm^{-1} and 634 cm^{-1} in the anodized sample, indicating the presence of anatase. In the plasma-oxidized sample, well-expressed bands are visible at 148 cm^{-1}, 242 cm^{-1}, 452 cm^{-1} and 618 cm^{-1}, indicating the presence of the rutile phase [34,35]. The Raman bands of rutile in the plasma-oxidized sample are more distinct than the anatase bands in the anodized sample. This can be attributed to several factors. Rutile typically has a higher Raman scattering cross-section, making its bands more intense. Another possible explanation is that the plasma oxidation process results in a more crystalline and phase-pure structure of rutile, which further increases the clarity and intensity of its Raman peaks compared to the anatase phase [36].

3.3. Electrochemical tests

The corrosion potential measurements and potentiodynamic curves are presented in Fig. 4 a and b, respectively. The electrochemical parameters extracted are given in Table 1.

During immersion in the physiological solution at 37 °C, the open circuit potential, E_{OCP}, of the reference Ti6Al4V was –0.162 V after 2 h immersion. The most positive E_{OCP} (+0.141 V) was measured in the anodized sample. A shift to more positive potentials in anodized Ti6Al4V surfaces in comparison to a non-treated surface has also been reported previously [37]. In the plasma-treated sample, the most negative E_{OCP} was –0.317 V. The shift towards the cathodic region in

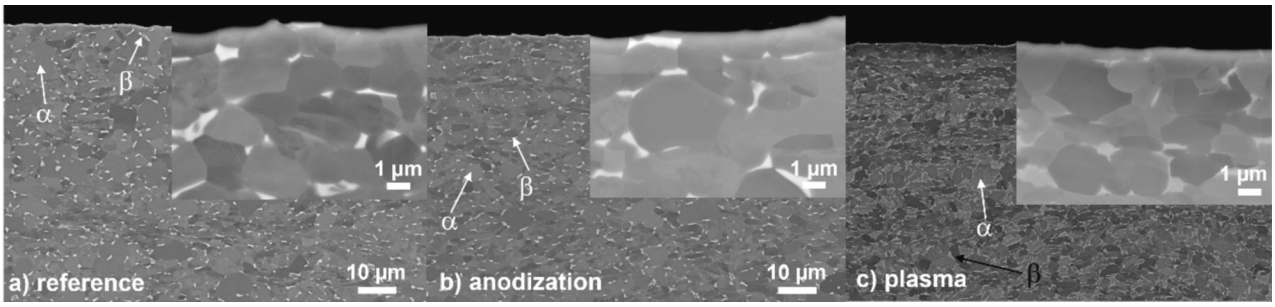

Fig. 1. Cross-sectional microstructures of the a) reference, b) anodized Ti6Al4V and c) plasma-treated specimens.

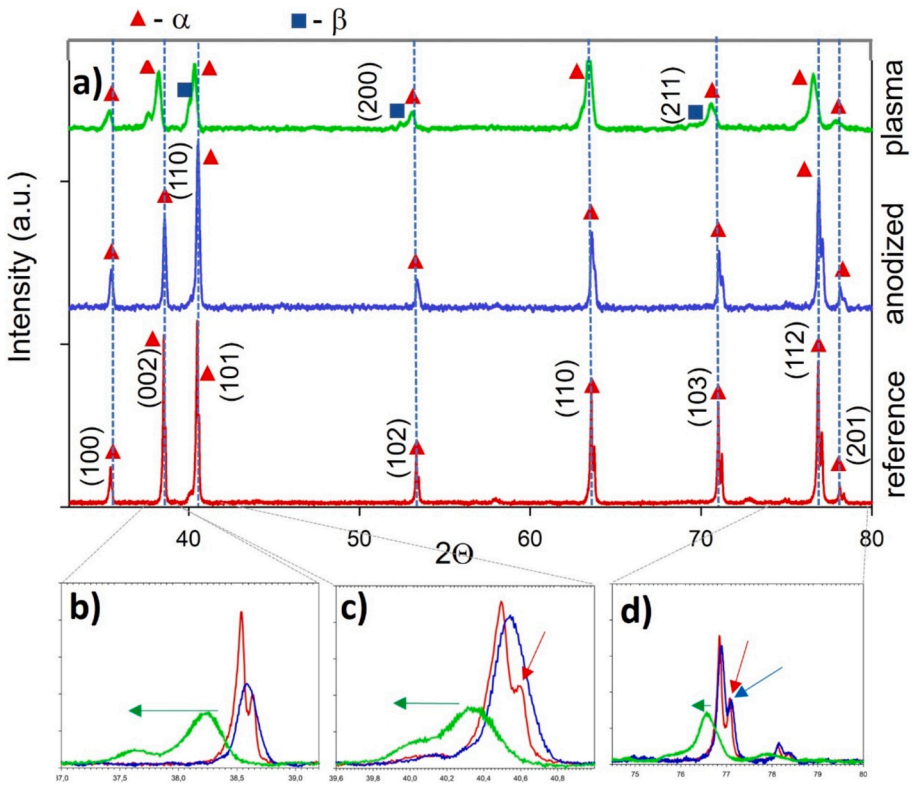

Fig. 2. XRD patterns of the reference, anodized, plasma-treated and laser-oxidized Ti6Al4V samples (a), with an enlarged view of the peaks for the hexagonal close packed (α) planes (002) (b), (101) (c) and (112) and (201) (d).

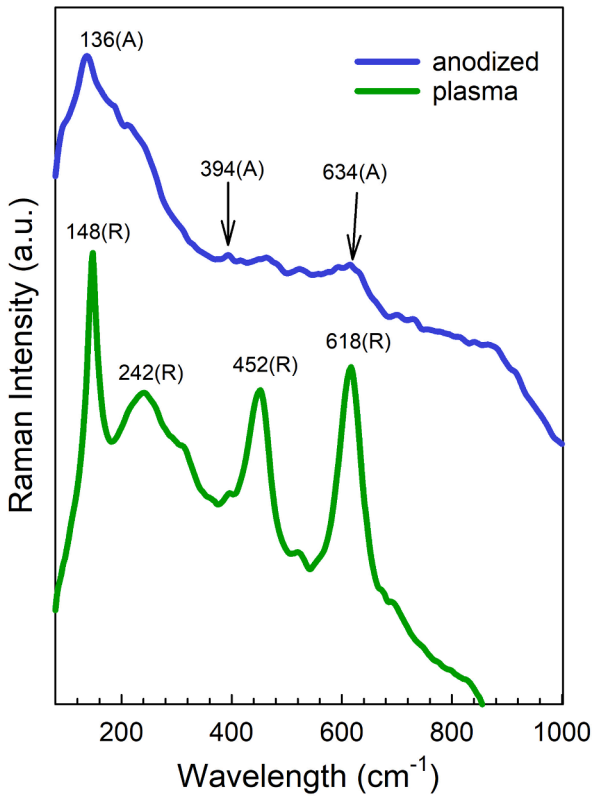

Fig. 3. Raman spectra for the anodised and plasma-oxidized Ti6Al4V alloys.

plasma-treated specimen indicates an increased anodic activity as compared to the reference and anodized specimens.

The passive behaviour of the differently-oxidized Ti6Al4V samples in the 0.9 wt% NaCl solution at 37 °C can be observed from the corrosion current densities, j_{corr}, and passive current densities, $j_{pass.}$ The transpassive potential, E_{trans}, is observed at potentials around 1.3 V, at which point a steeper increase in the current density is triggered, limited by a transpassive peak at 1.5 V (Table 1). The curves then extend into a second transpassive region, with different current density modes. ΔE, which is the difference between transpassive potential (E_{trans}) and corrosion potential (E_{corr}) presents a window of passivity – potential range during which the passive layer is stable. ΔE is the highest for reference specimen, if we neglect the j_{pass} slight increase and decrease at about 1.5 V.

The passive current density, j_{pass}, in the passive region is lower in the anodized specimen than in all the other samples tested, with a value of approximately 0.0365 μA/cm^2 (see Table 2). Of both the treated samples, those treated with plasma have the highest current density in the passive region (3.42 μA/cm^2). The corrosion properties are better in the reference sample than in the plasma-treated samples, since the lowest current densities were observed in potential ranges above 1.5 V (red curve). Polarization resistance was also defined from the potentiodynamic polarization tests, with the results shown in Table 2. Polarization resistance (R_p) is a measure of the resistance of a metallic material when transferring electrons to counterpart electroactive species present in a solution [38]. Here, the highest R_p was measured in the anodized samples, with the values for the reference specimens being approximately 4-times lower, and those for the plasma-treated specimen approximately 23-times lower. Similar results with respect to the preferential properties of anodized Ti6Al4V surfaces have been published previously [39].

Additionally, during the first week of exposure in 0.9 % NaCl, electrochemical impedance spectroscopy (EIS) tests were performed for each of the oxidized specimens and compared to the reference specimen. The tests were executed in a 0.9 wt% NaCl solution at 37 °C. The

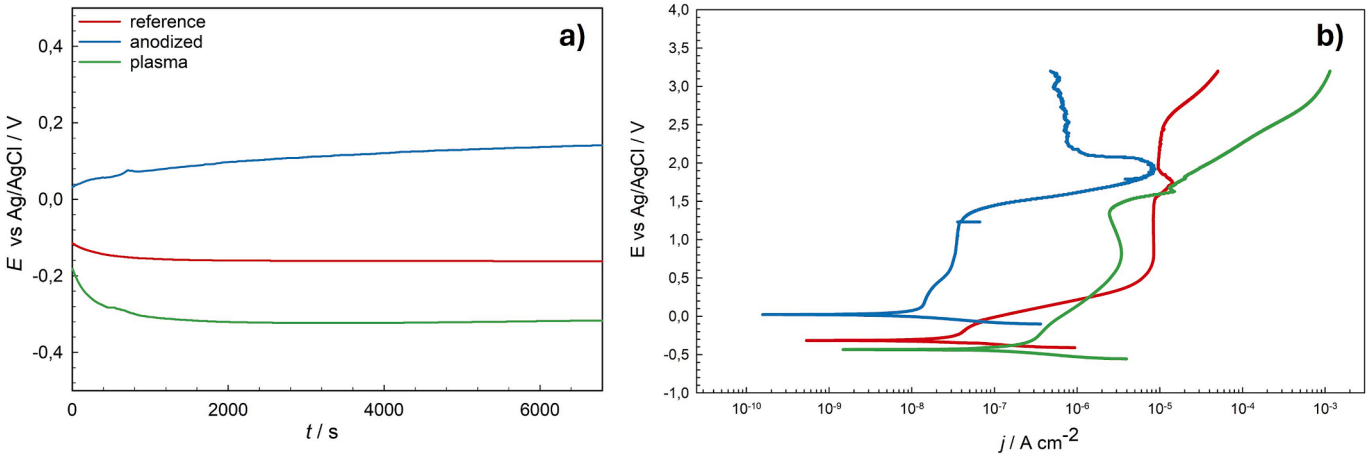

Fig. 4. Open circuit potential measurements (a) and potentiodynamic curves (b) for the reference Ti6Al4V, anodized and plazma-oxidized Ti6Al4V specimens.

Table 1
Parameters obtained from the electrochemical measurements.

		Reference Ti6Al4V	Anodised Ti6Al4V	Plasma treated Ti6Al4V
OCP	E_{corr} (V)	–0.12 ± 0.02	0.14 ± 0.06	–0.32 ± 0.02
PD	j_{corr} (nA/cm^2)	16.1 ± 7.21	11.8 ± 3.72	201 ± 16.1
	j_{pass} (μA/cm^2)	8.38	0.0365	3.42
	E_{trans} (V)	2.53 ± 0.02	1.27 ± 0.376	1.36 ± 0.025
	ΔE (E_{trans} – E_{corr}))(V)	2.65 ± 0.02	1.13 ± 0.41	1.68 ± 0.035
LP	R_p (MΩ cm^2)	2.73 ± 2.93	8.56 ± 3.19	0.37 ± 0.057

Table 2
Atomic concentrations of Ti, Al and V species at the outermost surface of the oxides (XPS depth profile at 0 nm) on the reference, anodized and plasma-treated specimens.

Specimen	Ti-oxide [at%]	Ti-metal [at%]	Al-oxide [at%]	Al-metal [at%]	V-oxide [at%]	V-metal [at%]
Reference Ti6Al4V	77.6	0.0	19.3	1.0	2.2	0.0
Anodised Ti6Al4V	89.3	0.0	10.2	0.3	0.3	0.0
Plasma treated Ti6Al4V	76.8	0.0	20.4	0.7	2.2	0.0

impedance spectra (Nyquist and Bode diagrams) are presented in Figure S1 in the Supplementary Information. EIS spectra were fitted with electrical equivalent circuits (EEC) using the ZView fitting program. The EIS response, represented as the sum of all resistances (R_p) in the EEC, apart from the solution resistance, during the 7 days of exposure, is presented in Fig. 5. The anodized specimen exhibited the highest R_p across the entire period of exposure, with a value of around 9.96 MΩ cm^2 at the end of the exposure. The second largest R_p (of 3.9 MΩ cm^2) was observed for the reference specimen. Polarization resistance, measured from the impedance spectra, was the lowest in the plasma-treated samples, with values of around 0.6 MΩ cm^2. These results coincide well with measurements deduced from the potentiodynamic tests.

3.4. Ion release test

The cumulative amounts of Al ions (left graph) and V ions (graph on the right side) released during 42 days of exposure to the 0.9 % NaCl solution are presented in Fig. 6. The amount shown for each day sampled is the sum of the amount from the previous sampling day (n-1) and the amount from the present sampling day (n). The rate of release of the Al ions slows after the 7th day of exposure, whereas the release rate for V ions is very slow during whole exposure – this pattern is observed in all specimens, with the exception of the specimen oxidized with plasma, where the ion release rate is significantly higher than for reference and anodized sample, and slow down after the 7th day of exposure. A complete cessation of ion release after an extended period of exposure was not observed in any of the specimens investigated. The cumulative amounts of ions released are low, reaching up to 0.04 μg/cm^2 for Al, and up to 0.4 μg/cm^2 for V. There are, however, some differences in results between the various specimens tested, which can be exposed and will be discussed later. The highest release of Al ions was observed in the reference specimen, with no artificial oxide layer, whilst the lowest release occurred in the anodized alloy. The amount of Al ions released from the plasma-treated specimen was similar to that seen in the reference alloy during the first week of exposure, but the release rate slowed down to the level of the anodized specimen for a period, before then rising again to become higher in comparison to the anodized specimen in the final week. With respect to the V ions released over the course of the test (right graph in Fig. 6), the total amount of ions released from the plasma specimen is a few times higher than both the reference alloy and the anodized specimen. As with Al, the rate of release rapidly increases during the first 4 days of exposure, then slows over the following weeks, but does not stop. The increase in the amount of V ions released between the first and last weeks of exposure is highest in the plasma-treated specimen and lowest in the reference specimen. In the anodized specimens, the rate increase of release of V ions is constant, from the beginning to the end of the test, but it is slow – together with the reference alloy this specimen exhibited the lowest total amount of V ions released at the end of the test.

3.5. SEM examination

Both before and after the ion release (immersion) test, the surfaces of the specimens were examined by SEM to observe any possible defects. The SEM images, together with true color optical images (shown as a small picture in the top left corner of each SEM image), are presented in Fig. 7. The surface of the reference Ti6Al4V specimen, with no artificial oxidation present, shows no visible change compared to the unexposed specimen, as can be seen in Fig. 7a. Before and after the immersion test, isohypsa-like lines are present on the surface of the α-grains, caused by the dissolution of this phase that occurred during milling, which was part of the sample preparation process. β-phase particles, with polygon-shaped edges, are evenly distributed across the surface. The particles

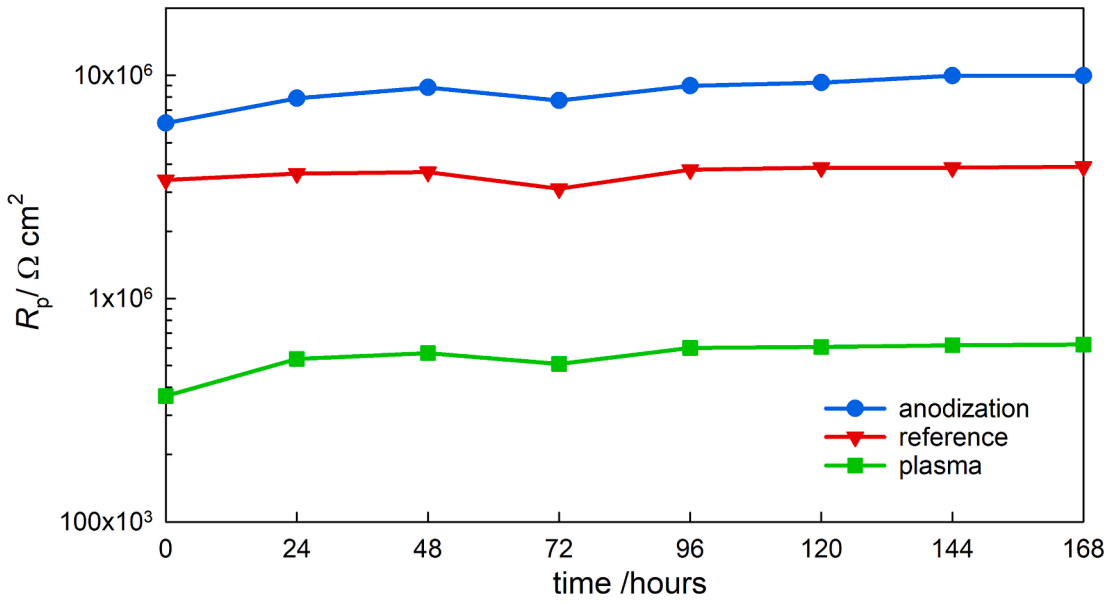

Fig. 5. Polarization resistance, presented as the sum of partial resistances, as obtained from EIS data, for the reference, anodized and plasma-treated Ti6Al4Al alloy specimens over the course of 1 week exposure to a 0.9 wt% NaCl solution at 37 °C.

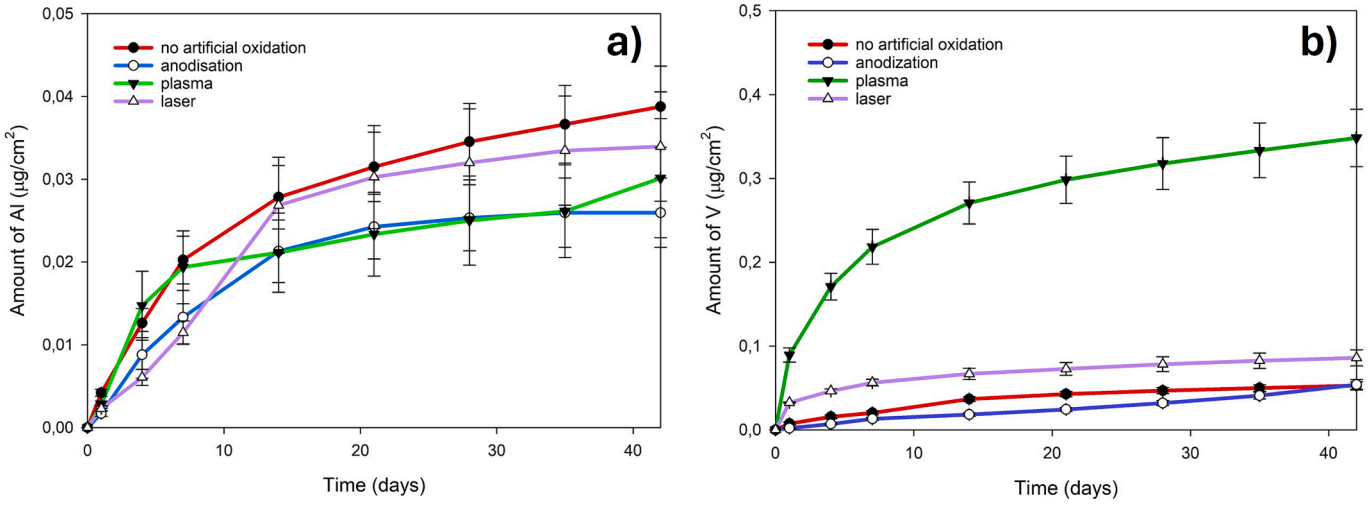

Fig. 6. Amounts of a) Al and b) V released during the immersion test.

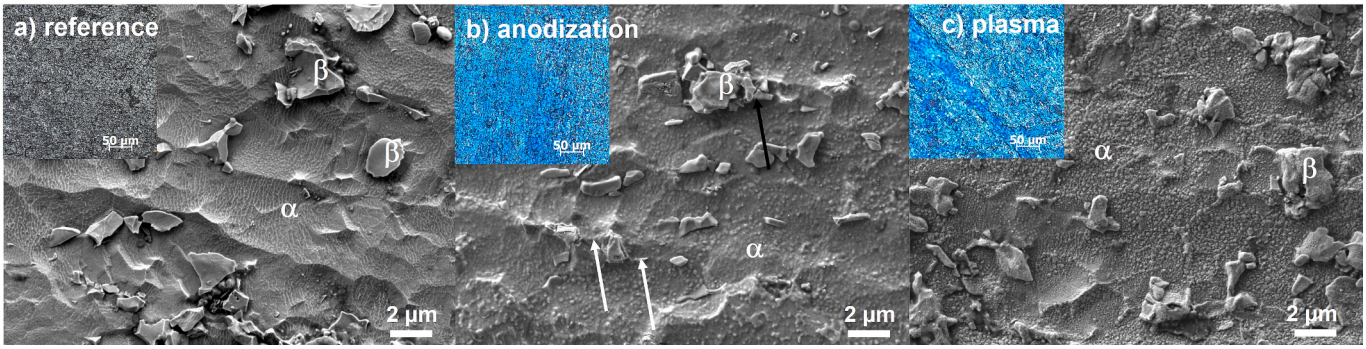

Fig. 7. SEM images and OM images (small images in the top left corner of each SEM image) of the a) reference, b) anodized, and c) plasma-treated specimen following the ion release test.

appear to be detached from the surface (undercut), which is likely due to the procedure used to clean the samples following their preparation in the ultrasonic bath. The anodized surface (Fig. 7b) is seemingly more smooth than the reference Ti6Al4V, with many bubble-like features on the α-phase that are not present on the β-phase. The edges of the β-phase in this specimen are smoother than on the reference specimen. Cracks are present on the upper surface of some of the β-phase (marked by the black arrow in the Fig. 7b). A few edges between the α and β-phases show the spalling of a film, most probably oxide formed by anodization (shown by the white arrows in the Figure Fig. 7b) after the ion release test. The surface of the Ti6Al4V oxidized in plasma (Fig. 7c) is covered with bubble-like features on the α-phase, similar to that seen on the anodized specimen, but denser. The density of the bubbles varies between individual α-phase grains, therefore it is assumed to be dependent on the grain orientation. No difference was observed between the surface of the plasma-treated specimen before and after the immersion test.

3.6. ToF-SIMS and XPS measurements

Fig. 8a, b and c show the SIMS depth profiles, measured in negative polarity, for the signals of TiO_2^-, AlO_2^- and VO^-, respectively. The intensities of the SIMS signals for each of the oxides on the reference, anodized and plasma-treated specimens are presented as a function of the oxide depth before and after the ion release test. The SIMS method is not quantitative, therefore the absolute concentration of these species cannot be determined, only their relative ratio. The thickness of the oxide films was evaluated where the TiO_2 signal crosses the TiAl signal in the SIMS depth profiles (see Supplementary information S2). The oxide thickness was 3 nm on the reference (non-treated) specimen, 42 nm on the anodized sample and 40 nm on the plasma-oxidized specimen. It follows that the thickness of the oxides on the two artificially-oxidized samples is similar, i.e. in the range 40–42 nm, giving them the blue surface color characteristic of a Ti-oxide of this thickness.

The reference, non-treated sample, is covered with a thin oxide layer containing Ti-oxide, Al-oxide and V-oxide. The intensity of all three of the oxides gradually decreases when moving from the surface of the oxide towards the oxide/ metal interlayer (red lines in Fig. 8).

In the anodized sample (shown by the blue lines in Fig. 8), Al-oxide and V-oxide are present in lower quantities at the oxide surface and the oxide/metal interface compared to the core of the oxide layer – the amounts gradually increase from both the outermost surface of the oxide and the metal/oxide interlayer towards the middle of the oxide. In the anodized samples, the largest amount of V-oxide was detected in the middle of the oxide layers, both before and after the ion release test. This means that V-oxide is trapped inside the oxide layer formed by anodization and is not released when immersed in the saline solution. At the outermost oxide surface, Ti-oxide enrichment is observed in comparison to the inner section of the oxide layer.

In the plasma-oxidized sample (green lines in Fig. 8), the Ti-oxide, Al-oxide and V-oxide are not distributed uniformly, but rather can be recognized as three layers. Al-oxide enriches the outermost surface of the oxide in a layer approximately 5 nm thick, and the interface between the metal and the oxide film to a depth of about 25 nm. The concentration of Al-oxide is lower in the middle of the oxide layer compared to on either side (i.e. at the outermost oxide surface and the metal/ oxide interface). In the inner section of the oxide layers, V-oxide is uniformly present. The largest V-oxide signal in the subsurface region (2–5 nm) in this sample was observed before the ion release test. After the ion release test the V-oxide signal in this region (black arrow in Fig. 8c) significantly decreased, corresponding to a pronounced release of V detected by the ion release test (Fig. 6b).

In addition to SIMS analyses, XPS depth analyses were also performed before the ion release test to quantitatively and qualitatively investigate any differences in the structure of the oxide layer between the anodized and plasma-treated specimens. XPS spectra, Ti $2p_{3/2}$ and Al $2p_{3/2}$ were related with Ti(4 +) and Al(3 +) oxidation states at 458.6 eV and 74.0 eV, confirming the presence of the oxides TiO_2 and Al_2O_3 on the surface, as expected [40]. Following the acquisition of XPS spectra on the surface of all the samples, depth profiling was performed. The shape of the Ti 2p, Al 2p, and V 2p spectra changed significantly during depth profiling, indicating a transition from Ti-oxide, Al-oxide, and V-oxide towards Ti-metal, Al-metal and V-metal. This spectral change can be explored to follow how specific oxides are distributed within the oxide layer. We applied the method known as “linear least square fitting” (LLS), available in the Multipak processing software, through which every single spectrum obtained at a certain depth was decomposed into a Ti-oxide peak at 458.6 eV, a Ti-metal peak at 454.0 eV, an Al-oxide peak at 74.0 eV, an Al-metal peak at 72.0 eV, a V-oxide peak at 515.0 eV and a V-metal peak at 511.0 eV. In this way, six curves were obtained for Ti, Al and V as a function of depth. XPS depth profiles of the relative concentration of different types of cations (Ti-oxide, Ti-metal, V-metal, Al-oxide, Al-metal, V-oxide) are presented in Fig. 9. The solid lines correspond to the relative concentration of oxides versus depth, while the dotted lines represent the relative concentrations of the metallic components, Ti, Al and V. These XPS depth profiles allow quantitative aspects of the oxide layers to be determined, which is not possible from the SIMS depth profiles. The SIMS depth profiles (Fig. 8), on the other hand, have better depth resolution and chemical sensitivity, allowing the depth distribution of components in the oxide layers to be followed more precisely. The atomic concentrations of Ti-oxide, Ti-metal, Al-oxide, Al-metal, V-oxide and V-metal at the outermost surface of all three specimens are presented in Table 2. The XPS profiles for the reference Ti6Al4V specimen (Fig. 9a and b) and the plasma specimen (Fig. 9e and f) show an enrichment of Al-oxide and V-oxide, and a deficit of Ti-oxide, at the outermost surface. The atomic concentration of Ti oxide increases slightly between the outermost surface and the metal interface, reaching its maximum value at a depth of approximately 2 nm in the reference specimen, and at 5 nm in the plasma specimen. The amount of V-oxide in the oxide layer of the reference specimen reaches a maximum (of approximately 3.7 at.%) at around 1.5 nm below the outer surface (Fig. 9a and b), and decreases nearer the metallic surface. In the reference specimen, the concentration of Al-oxide reached its maximum at the outermost surface, then decreased from that point moving towards the surface of the metal. Fig. 9e and f show the enrichment of Al-oxide at both the outermost surface and the oxide/metal interface in the plasma-treated samples. On the contrary, V-oxide is not present in the outermost layer in the anodized specimen (to about 5 nm; Fig. 9c and d), although Al-oxide is seen to be uniformly distributed across the outermost 30 nm of this specimen.

We should note that a possible explanation for changing the chemical states of Ti from Ti(4 +) to metallic Ti described above might also be a preferential sputtering by Ar bombardment showing the reduction of Ti (4 +) to Ti (2+/3 +) states. This artefact was often observed during the Ar-sputtering of Ti-oxide layers [41]. We decomposed Ti 2p spectra taken during the depth profile using the LLS method (Fig. 9a, c, e) into the surface TiO2-like spectrum and the Ti-metallic spectrum from the base alloy. Therefore, we supposed that Ti(2+/3 +) states possibly formed due to preferential sputtering did not significantly influence the profile curves for Ti-oxide and Ti-metallic species.

4. Discussion

Results from the electrochemical tests conducted in 0.9 wt% NaCl, presented in section 3.3, shows that oxidation of the Ti6Al4V alloy did not always improve its corrosion resistance. Oxidation by anodization significantly improved (increased) polarization resistance (a measure of corrosion resistance) in comparison to the reference specimen. The plasma-treated specimen, on the other hand, had the lowest polarization resistance of all the specimens investigated.

During the ion release test, both types of oxidation processes investigated suppressed the release of Al into the 0.9 wt% NaCl solution. The amount of Al ions released from the anodized and plasma-oxidised

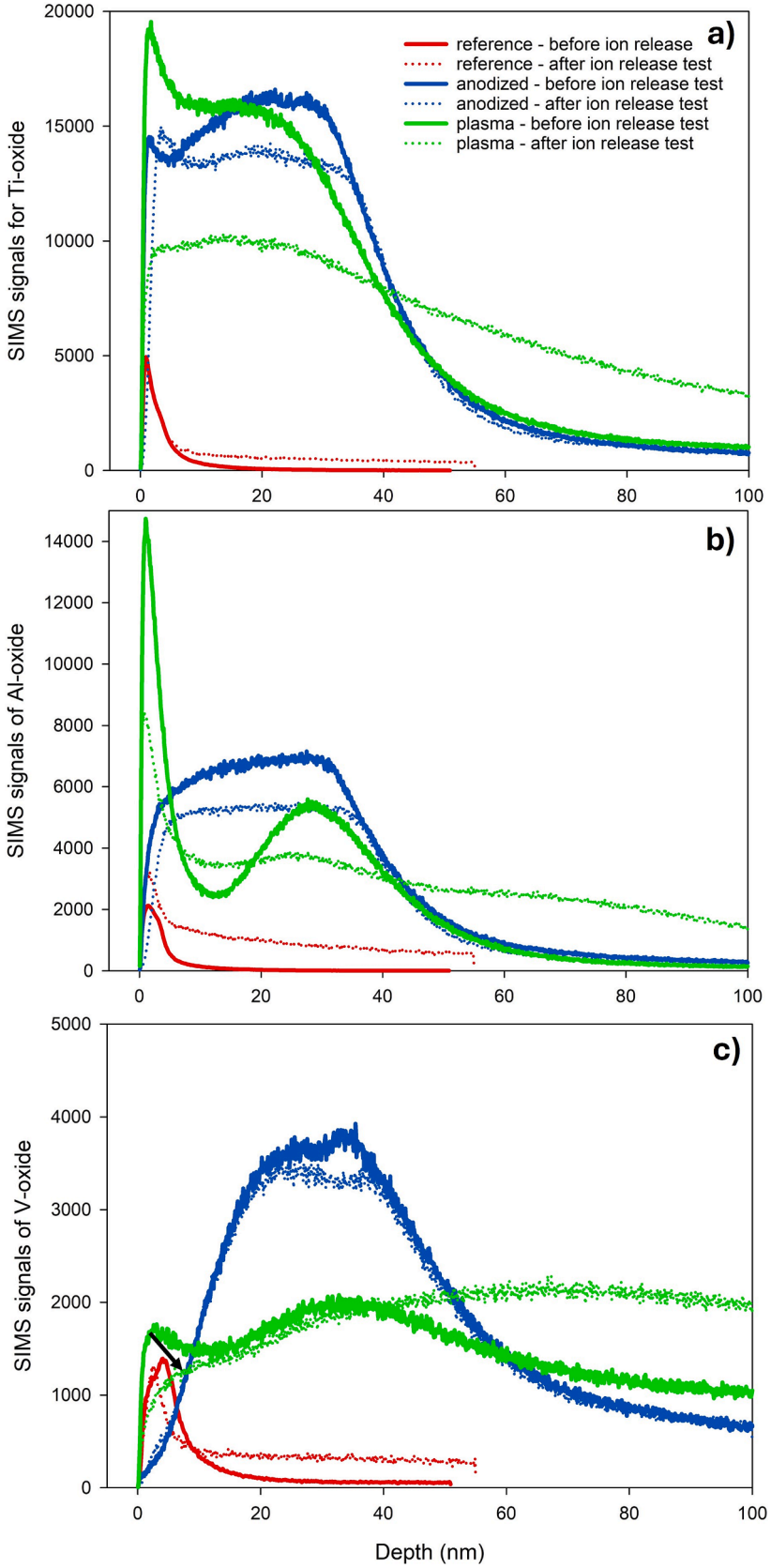

Fig. 8. Intensities of the SIMS signals of titanium oxide (TiO_2^-), a fragment of aluminium oxide (AlO_2^-) and a fragment of vanadium oxide (VO^-) as a function of depth, before and after the 42 days of ion release test, for the reference, anodized and plasma-treated specimens.

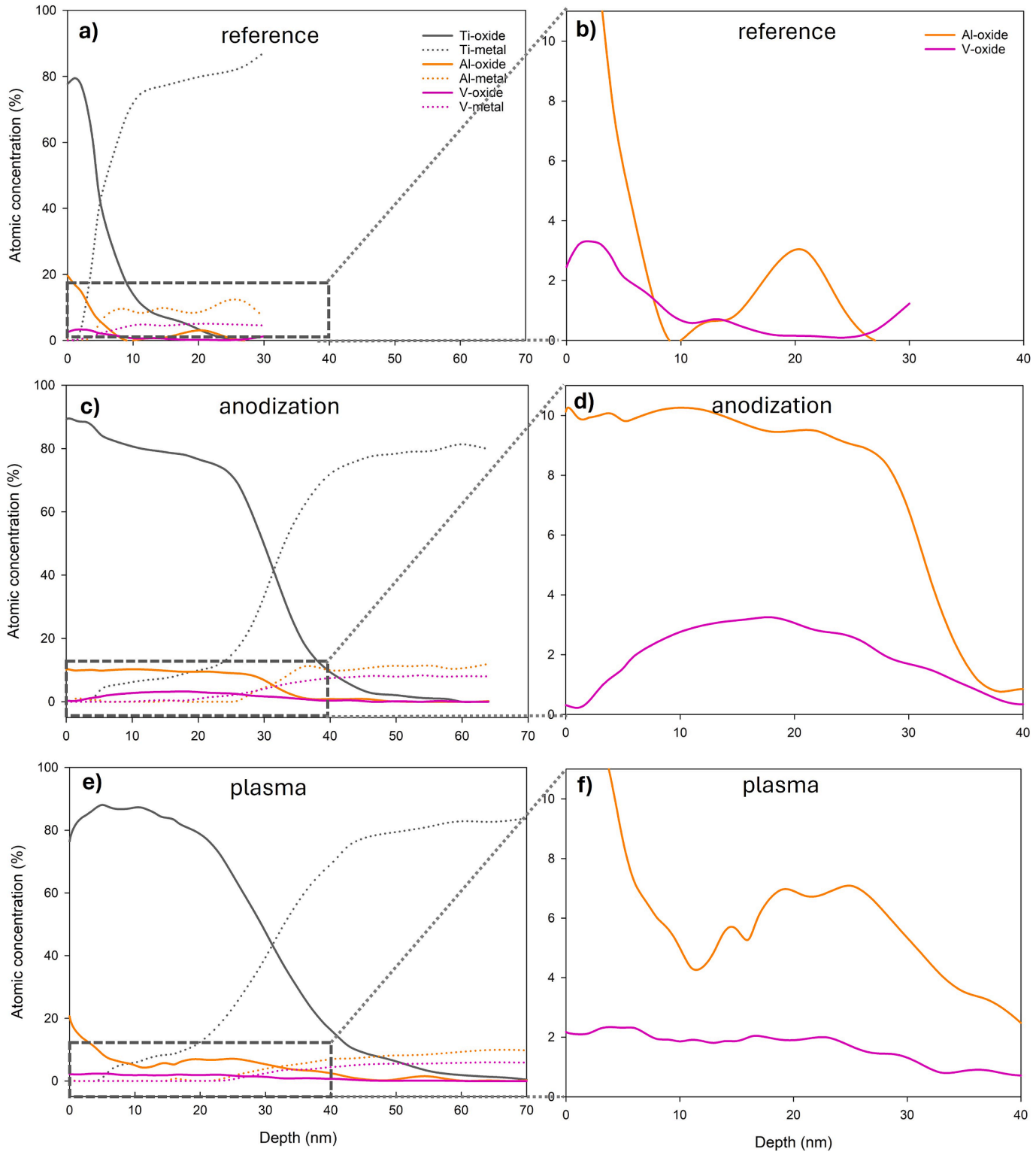

Fig. 9. Full XPS depth profiles of Ti-oxide, Ti-metal, Al-oxide, Al-metal, V-oxide and V-metal for the (a) reference, (c) anodized and (e) plasma-treated specimens, and enlarged Al-oxide and V-oxide profiles for the (b) reference, (d) anodized and (f) plasma-treated specimens.

specimens was very similar. During the same test, no significant difference was observed between the amount of V released from the reference and anodized specimens. The amount of V released from the plasma-treated specimen, on the other hand, was a few times higher.

This finding led to an in-depth analysis of the oxides, investigating the differences in their composition and structure, which are believed to have a crucial influence on corrosion behavior during exposure to a saline environment. Differences in the thickness of the oxide in the artificially-oxidized, anodized (42 nm) and plasma-treated (40 nm) specimens did not significantly influence the corrosion resistance in 0.9 % NaCl. Indeed, the influence of the thickness of the oxide layer on titanium alloys, produced either by thermal oxidation, or electrochemically, has been extensively studied previously [25,42,43], with a general increase in corrosion resistance seen as the thickness of the oxide layer

increases. In the case of electrochemical anodization, increasing the applied voltage increases the thickness of the oxide. In most cases this has been shown to improve corrosion resistance, the exception to this being when the oxide formed is porous [42,44]. With thermal oxidation, both the thickness of the oxide and the corrosion resistance increase as the process temperature is increased [42]. The limitation of these studies, however, is that while they compare the corrosion resistance of oxide layers of differing thicknesses, these oxides are only generated by one type of oxidation – thus the influence of the type of oxidation on corrosion behavior is not considered. Namely, the compositional variation of an oxide layer grown electrochemically (i.e. through anodization) is different from that of one grown thermally (i.e. through plasma treatment).

4.1. Thermal oxidation

The standard Gibbs free energies (ΔG^{o}_{T}, equation (1)) for the formation of oxides on Ti6Al4V in a thermally oxidized layer, according to the oxidation reactions (2), (3) and (4), are -960.76 kJmol^{-1} for TiO_2, -1146.76 kJmol^{-1} for Al_2O_3 and -872.96 kJmol^{-1} for V_2O_3 [45,46].

$$\Delta G^{o}_{T} = \Delta H^{o}_{298} - T \bullet \Delta S^{o}_{298} \quad (1)$$

$$Ti + O_2 = TiO_2 \quad (2)$$

$$4Al + 3O_2 = 2Al_2O_3 \quad (3)$$

$$4V + 5O_2 = 2V_2O_5 \quad (4)$$

The more negative the standard Gibbs energy, the higher the feasibility of oxide formation. In titanium alloys, however, titanium oxidizes preferentially to the other alloying elements. The passive film of a Ti-alloy is an n-type semiconductor [8,47,48], which grows inward. The partial oxygen pressure in the oxide decreases from the outermost surface of the oxide towards the oxide/metal interface, where the oxygen reacts with the titanium in Ti6Al4V to form TiO_2. At the oxide/metal interface, the activity of Al is reduced by V and therefore Al_2O_3 cannot be formed. Al from the metal diffuses through the oxide to its outermost surface, where it reacts with oxygen and forms Al_2O_3 [32,49]. Vanadium oxides (such as V_2O_5) are also not formed at this interface due to low oxidation rate. The vanadium eventually oxidizes when it reaches the outer surface, but this oxidation primarily occurs at the outermost layer, due to the lower oxygen affinity and higher mobility of vanadium compared to titanium and aluminum.

4.2. Electrochemical oxidation

The thickness of an anodic oxide film on a titanium alloy depends on the anodic voltage, while its morphology primarily depends on the type of titanium alloy, the anodization time and the anodizing electrolyte [50]. The ToF SIMS and XPS analysis conducted in this research show that the distribution of Ti, Al and V oxides within the anodized layer can be described by the oxidation mechanism outlined in Yamagami et. al. [51], characterized as follows: 1) early stage of anodization, during which negatively charged anions and oxide ions move to the metal surface, which acts as an anode; 2) middle stage, with the occurrence of a double electron layer – the outer layer contains Ti^{4+} ions, and the inner layer near metal contains Ti^{4+}, Al^{3+} and V^{5+} ions. As a result, the inner layer contains Ti, Al, V and oxygen, while only Ti and oxygen are present in the outer layer.

4.3. Structure of the oxide layers

The ToF-SIMS depth analysis and XPS depth profiles revealed some differences in the distribution and quantity of the Ti-, Al- and V-oxides within the oxide layer between the specimens examined before and after the ion release test. With both methods, the oxide layer formed by anodization shows a high Ti-oxide/Al-oxide ratio and a high Ti-oxide/V-oxide ratio at the outermost surface. The SIMS signals for Al-oxide and V- oxide increase when moving from the oxide surface towards the oxide/metal interlayer, from zero at an oxide depth of 5 nm to an almost constant value at a depth of 20 nm (Fig. 8b and c, respectively).

As can be seen from the enlarged XPS profiles for the reference, anodized and plasma-treated specimens, presented in Fig. 9b, d and f, respectively, the atomic concentrations of Al-oxide and V-oxide vary significantly at the outermost oxide surface. The concentration of Al-oxide at the surface was twice as high in the plasma-treated specimen, whilst the concentration of V-oxide was more than 7-times higher. Similar observations were made for the reference specimen. As a result, the concentration of Ti-oxide at the surface is lower in the reference and plasma-treated specimens than in the anodized sample.

Table 2 indicates the presence of a certain amount of Al oxide on the anodized surface before the ion release test, but its atomic concentration was only half that of the plasma-treated surface. ToF SIMS and XPS analyses show that Al-oxide and V-oxide are already present in the outermost layer in the plasma specimens. As this surface is in contact with the environment, it causes release of these two constituents.

4.4. Crystallographic properties of the oxide layers

Raman spectroscopy showed that the oxide formed by anodization is mainly anatase, while the oxide formed by plasma is mainly rutile. It can be deduced from the broad shape of the Raman bands that neither of the oxides investigated are fully crystalline [44]. Both oxide forms have a tetragonal close packed structure, with one titanium atom surrounded by six oxygen atoms to form an octahedral coordination. The rutile structure, however, is denser than anatase, making it more thermally stable and improving the corrosion resistance according to the literature [25,52]. Rutile was identified in the plasma-treated samples. This is due to thermal oxidation in the plasma process. Here, the core is heated inductively through thermal conductivity, causing an increase in the temperature at the surface. Thermal oxidation is, however, limited, due to the low partial pressure of oxygen in a vacuum. Despite this, oxygen diffuses into the interstitial sites of the titanium lattice below the surface [53,54], thus increasing the hardness (see Table S2). The present study investigated the corrosion properties, structure and crystallinity of oxides on a Ti6Al4V alloy in order to compare those grown electrochemically and thermally. Although it has been reported in the literature that rutile is more corrosion resistant than anatase, this claim was not related to the structure of an oxide film, as was investigated in this study. Results of this study suggests that there is not a clear correlation between corrosion resistance and christallography of the oxide of Ti6Al4V.

4.5. Corrosion and biocompatibility properties of oxide layers on Ti6Al4V

When Ti6Al4V is exposed to a corrosive media, Ti, Al and V ions are released into the solution. In a 0.9 % NaCl solution, Cl^- ions cause an autocatalytic process, which includes the adsorption of Cl^- to the oxide surface and its combination with oxygen vacancies into an oxide film [55]. This enables the formation of oxygen ions and their transport to the metal/oxide interface, which slows down or even stops the formation of the oxide layer, while at the same time accelerating the formation of more oxygen vacancies and their recombination with chloride ions. This, in turn, accelerates the formation of titanium ion vacancies, which then migrate towards the metal/oxide surface. Here they cannot annihilate, so they condense, causing the thinning and eventual breakdown of the oxide layer [8,55,56]. The same process simultaneously occurs for Al- and V-oxides, but V-oxide is less stable than Al-oxide (and Ti-oxide), so if it is present in the outer layer it is preferentially dissolved. Following the ion release test, the biggest drop in the V-oxide concentration of the oxide on the plasma-treated specimen occurred in the outermost layer (see Fig. 8c), where the highest deficiency was seen in

comparison to its initial state (i.e. before the ion release test), suggesting that the 'difference' had migrated into the solution. This was confirmed by the increased concentration of V in the ion release test (Fig. 6b). Although the atomic concentrations of V-oxide in the outermost oxide layers of the reference and plasma-treated specimens is similar (Table 2), the release of V from the plasma-treated specimen is significantly higher. Furthermore, the polarization resistance in the long-term EIS test (Fig. 5) is 6 times lower in the plasma-treated specimen than in the reference Ti6Al4V. Corrosion current density (j_{corr}) is also highest for the plasma-treated specimen (Table 1, Fig. 4). Together this provides clear evidence that the plasma-treated oxide layer offers poor protection in comparison to the reference Ti6Al4V.

In the case of the anodized specimen, vanadium oxide was shown to be absent from the outermost surface in the present study, as has been also reported in previous studies [8,57,58]. The significant new observation is that the difference in the amount of V present in the outermost oxide layer of the anodized and plasma-treated Ti6Al4V alloy is crucial for their ion release (biocompatibility) and corrosion properties.

Corrosion properties are governed by the presence of Al-oxide and V-oxide within the Ti-oxide layer. V-oxide is known to be less stable than Ti- and Al-oxides [7,8] when in contact with media containing chloride [55]. Its presence in the alloy and oxide, together with the presence of Al, generates different point defects due to difference in valence [55]. The differences between the ionic and covalent radii of V and Ti are an additional reason for the increased concentration of point defects [8] and destabilization of the oxide.

The present study determined that the outermost oxide layer of plasma treated and reference specimens was enriched with Al-oxide and V-oxide. At the same time, only Al-oxide enrichment has been reported previously [41]. As observed in our study, simultaneous enrichment with V-oxide on the plasma-treated (oxidized) and reference Ti6Al4V has yet to be reported. This enrichment caused an increase in the release of vanadium ions from plasma-treated specimens but not from reference specimens. The extent of vanadium enrichment substantially differs between the oxides formed electrochemically (anodization) and thermally (plasma). EIS measurements and subsequent fitting of the results (results for EIS presented in supplementary file, Figure S1) showed different properties of investigated oxide films on reference, anodized, and plasma-treated specimens. Oxide on reference Ti6Al4V specimen is thin and compact; anodized sample oxide is thicker and composed of the compact barrier layer and slightly porous outer layer. In contrast, plasma specimen oxide is substantially different, with a less protective barrier film and a very porous and full of defects outer layer. This was reflected in the equivalent circuits that fit the impedance results (see Figure S1 and Table S1). The summarized properties of electrochemical investigation, ion release tests and characterization of oxide layers are schematically presented in Fig. 10. The tentative model in Fig. 10 demonstrates that the oxide layer on plasma-treated and reference Ti6Al4V specimens is enriched with both Al-oxide and V-oxide; however, as derived from EIS measurements and fitting results, the plasma-treated oxide layer is highly porous and defective compared to the compact oxide on the reference specimen which causes release of increased amount of V into testing solution. On the other hand, anodized specimen oxide is V- free and contains fewer defects at the outermost surface in comparison to plasma-treated specimen, which leads to its overall better performance.

5. Conclusion

In this study, blue oxides formed on a Ti6Al4V alloy were compared using electrochemical methods, ion release tests and various spectroscopic techniques in a 0.9 % NaCl solution at body temperature.

The thermal oxidation process (i.e. plasma treatment) is substantially different from the electrochemical oxidation process (i.e. anodization), which is reflected in the electrochemical processes, ion release and structure of the oxide layer.

The oxide layer formed by plasma, which is thermal oxidation process, was 40 nm thick and consisted of an outer layer containing V- and Al-oxide, in addition to Ti-oxide, and Al-oxide enrichment at the metal-oxide interface. The electrochemical parameters showed that this oxide is porous with lower protective properties, while the high release of V ions indicated lower biocompatibility.

The oxide layer formed by anodization was 42 nm thick and consisted of all three oxides, with the outermost layer enriched with Ti- and Al-oxide. This oxide exhibited the highest polarization resistance and lowest corrosion current density, showing its superior corrosion resistance. This was further confirmed by the lower amounts of Al and V released.

Relying on a single type of investigation, such as electrochemical or spectroscopic analysis, to conclude the protective properties of oxides can be misleading. Further exploration into the defects of oxides would unquestionably enhance the understanding of the corrosion and protective properties of oxide layers in a Ti6Al4V alloy.

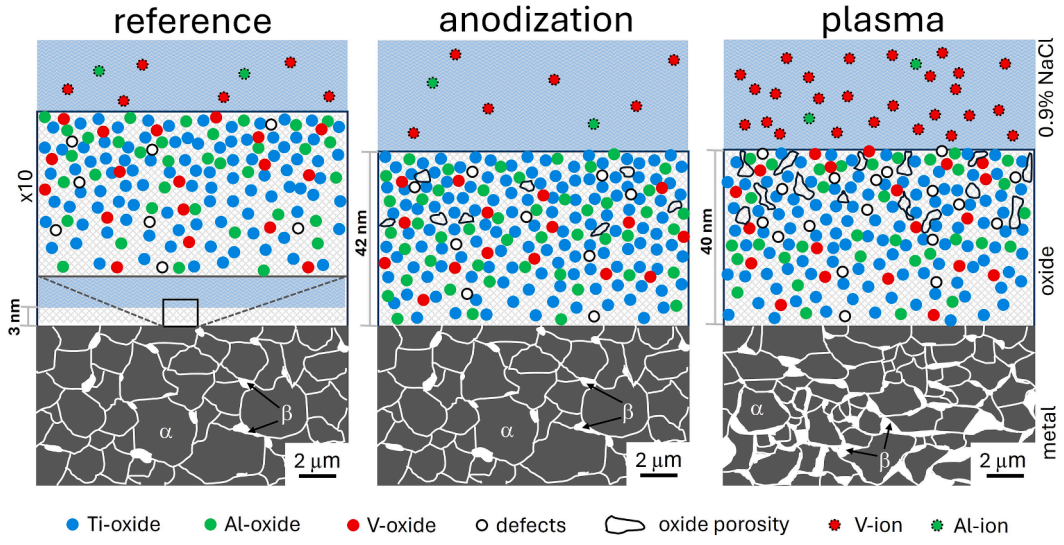

Fig. 10. Schematic view of oxide structures and ions migration into 0.9% NaCl.

CRediT authorship contribution statement

Mirjam Bajt Leban: Writing – review & editing, Writing – original draft, Methodology, Investigation, Formal analysis, Conceptualization. **Tadeja Kosec:** Writing – review & editing, Writing – original draft, Methodology, Investigation, Formal analysis. **Aleksandra Kocijan:** Writing – original draft, Formal analysis. **Marjetka Conradi:** Writing – original draft, Formal analysis. **Ita Junkar:** Writing – original draft, Formal analysis. **Janez Kovač:** Writing – original draft, Formal analysis.

Declaration of competing interest

The authors declare that they have no known competing financial interests or personal relationships that could have appeared to influence the work reported in this paper.

Acknowledgments

This paper was financed by the Slovenian Research Agency through the core research programs P2-0082, P2-0273 and P2-0132 and research projects L2-4445 and J3-4502.

Data availability.

The data that support the findings of this study are available from the corresponding authors upon reasonable request.

Appendix A. Supplementary data

Supplementary data to this article can be found online at https://doi.org/10.1016/j.apsusc.2024.161486.

Data availability

Data will be made available on request.

References

[1] M.Q. Francis, H. Froes, Titanium in medical and dental applications, Elsevier (2018), https://doi.org/10.1016/C2016-0-03591-X.
[2] D.M. Brunette, P. Tengvall, M. Textor, P. Thomsen, Titanium in Medicine: Material Science, Surface Science, Engineering, Biological Responses and Medical Applications, Springer, Berlin Heidelberg, Berlin, Heidelberg (2001), https://doi.org/10.1007/978-3-642-56486-4.
[3] W. Ahmed, M.J. Jackson, eds., Surgical Tools and Medical Devices, Springer International Publishing, Cham, 2016. https://doi.org/10.1007/978-3-319-33489-9.
[4] C. Leyens, M. Peters, eds., Titanium and titanium alloys: fundamentals and applications, Wiley-VCH ; John Wiley] (distributor), Weinheim : [Chichester, 2003.
[5] P. Pushp, S.M. Dasharath, C. Arati, Classification and applications of titanium and its alloys, Materials Today: Proceedings 54 (2022) 537–542. https://doi.org/10.1016/j.matpr.2022.01.008.
[6] M.J. Donachie, Titanium: a technical guide, 2nd ed, ASM International, Materials Park, OH, 2000.
[7] M. Bajt Leban, T. Kosec, M. Finšgar, The corrosion resistance of dental Ti6Al4V with differing microstructures in oral environments, J. Mater. Res. Technol. 27 (2023) 1982–1995, https://doi.org/10.1016/j.jmrt.2023.10.082.
[8] M. Metikoš-Huković, A. Kwokal, J. Piljac, The influence of niobium and vanadium on passivity of titanium-based implants in physiological solution, Biomaterials 24 (2003) 3765–3775, https://doi.org/10.1016/S0142-9612(03)00252-7.
[9] P. Bocchetta, L.-Y. Chen, J.D.C. Tardelli, A.C. dos Reis, F. Almeraya-Calderón, P. Leo, Passive Layers and Corrosion Resistance of Biomedical Ti-6Al-4V and β-Ti Alloys, Coatings 11 (2021) 487, https://doi.org/10.3390/coatings11050487.
[10] S. Shelly, S. Liraz Zaltsman, O. Ben-Gal, A. Dayan, I. Ganmore, C. Shemesh, D. Atrakchi, S. Garra, O. Ravid, D. Rand, H. Israelov, T. Alon, G. Lichtenstein, S. Sharabi, D. Last, F. Gosselet, V. Rosen, G. Burstein, A. Friedlander, R. Harel, G. Vogel, M. Schnaider Beeri, Y. Mardor, Y. Lampl, G. Fleminger, I. Cooper, Potential neurotoxicity of titanium implants: Prospective, in-vivo and in-vitro study, Biomaterials 276 (2021) 121039, https://doi.org/10.1016/j.biomaterials.2021.121039.
[11] E. Fuentes, S. Alves, A. López-Ortega, L. Mendizabal, V.S. de Viteri, E. Fuentes, S. Alves, A. López-Ortega, L. Mendizabal, V.S. de Viteri, Advanced Surface Treatments on Titanium and Titanium Alloys Focused on Electrochemical and Physical Technologies for Biomedical Applications, in: Biomaterial-Supported Tissue Reconstruction or Regeneration, IntechOpen, 2019. https://doi.org/10.5772/intechopen.85095.
[12] H. Dong, Surface engineering of light alloys: aluminium, magnesium and titanium alloys, CRC Press, Boca Raton (fla.) (2010).
[13] M.V. Diamanti, B. Del Curto, M. Pedeferri, Anodic Oxidation of Titanium: From Technical Aspects to Biomedical Applications, J. Appl. Biomater. Biomech. 9 (2011) 55–69, https://doi.org/10.5301/JABB.2011.7429.
[14] R. Dalmis, O. Yılmaz, T. Dikici, A new concept for the eco-friendly structural colorization of anodic titania: Photonic crystal structure, Colloids Surf A Physicochem Eng Asp 631 (2021) 127748, https://doi.org/10.1016/j.colsurfa.2021.127748.
[15] IOM3, Interference Colours on Titanium: From Science to Art, (n.d.). https://www.iom3.org/resource/interference-colours-on-titanium-from-science-to-art.html (accessed November 9, 2023).
[16] P. Chandramohan, R. Raghu, B. Ravisankar, Anodizing and its effects on mechanical properties and corrosion resistance of laser additive manufactured Ti-6Al-4V alloy, Int. J. Mater. Res. 111 (2020) 654–660, https://doi.org/10.3139/146.111931.
[17] M. Benčina, N. Rawat, K. Lakota, S. Sodin-Šemrl, A. Iglič, I. Junkar, Bio-performance of hydrothermally and plasma-treated titanium: the new generation of vascular stents, Int. J. Mol. Sci. 22 (2021), https://doi.org/10.3390/ijms222111858.
[18] M. Benčina, I. Junkar, R. Zaplotnik, M. Valant, A. Iglič, M. Mozetič, Plasma-induced crystallization of TiO_2 nanotubes, Materials 12 (2019) 626, https://doi.org/10.3390/ma12040626.
[19] I. Junkar, A. Iglič, J. Kovač, M. Mozetič, M. Kulkarni, Method for coating a medical device, especially a vascular stent, WO2018029166A1 (2018).
[20] I. Junkar, M. Kulkarni, B. Drašler, N. Rugelj, N. Recek, D. Drobne, J. Kovač, P. Humpolicek, A. Iglič, M. Mozetič, Enhanced biocompatibility of TiO_2 surfaces by highly reactive plasma, J. Phys. D: Appl. Phys. 49 (2016) 244002, https://doi.org/10.1088/0022-3727/49/24/244002.
[21] M.A. Hussein, A. Madhan Kumar, A.F. Abdelaal, M. Abdul Azeem, Surface Analysis and In Vitro Corrosion Properties in Artificial Saliva of Surface-Treated Ti6Al4V Alloy for Dental Applications, Metall Mater Trans A 52 (2021) 4299–4309, https://doi.org/10.1007/s11661-021-06387-2.
[22] D.A.H. Hanaor, C.C. Sorrell, Review of the anatase to rutile phase transformation, J Mater Sci 46 (2011) 855–874, https://doi.org/10.1007/s10853-010-5113-0.
[23] V.S. De Viteri, R. Bayón, A. Igartua, G. Barandika, J.E. Moreno, C.-P.-J. Peremarch, M.M. Pérez, Structure, tribocorrosion and biocide characterization of Ca, P and I containing TiO2 coatings developed by plasma electrolytic oxidation, Appl. Surf. Sci. 367 (2016) 1–10, https://doi.org/10.1016/j.apsusc.2016.01.145.
[24] B. Li, L. Zhang, Y. Li, H. Li, L. Zhou, C. Liang, H. Wang, Corrosion Resistance and Biological Properties of Anatase and Rutile Coatings on a Titanium Surface, Chem. Lett. 48 (2019) 1355–1357, https://doi.org/10.1246/cl.190549.
[25] J. Birch, T. Burleigh, Oxides Formed on Titanium by Polishing, Etching, Anodizing, or Thermal Oxidizing, Corrosion 56 (2000), https://doi.org/10.5006/1.3280511.
[26] B. Minhas, S. Dino, Y. Zuo, H. Qian, X. Zhao, Improvement of Corrosion Resistance of TiO2 Layers in Strong Acidic Solutions by Anodizing and Thermal Oxidation Treatment, Materials (basel) 14 (2021) 1188, https://doi.org/10.3390/ma14051188.
[27] R.J.D. Tilley, Colour and the optical properties of materials: an exploration of the relationship between light, the optical properties of materials and colour, 2nd ed, Wiley, Hoboken, N.J., 2011.
[28] M.V. Diamanti, B. Del Curto, M. Pedeferri, Interference colors of thin oxide layers on titanium, Color Res. Appl. 33 (2008) 221–228, https://doi.org/10.1002/col.20403.
[29] K. Płacheta, A. Kot, J. Banas-Gac, M. Zając, M. Sikora, M. Radecka, K. Zakrzewska, Evolution of surface properties of titanium oxide thin films, Appl. Surf. Sci. 608 (2023) 155046, https://doi.org/10.1016/j.apsusc.2022.155046.
[30] V. Ducros, M. Peoc'h, C. Moulin, D. Ruffieux, J. Amossé, A. Favier, B. Pasquier, Titanium identification and measurement by ICP-MS and ICP-OES in a human spleen fragment, Clin. Chem. 42 (1996) 1875–1877, https://doi.org/10.1093/clinchem/42.11.1875.
[31] J.F. Moulder, W.F. Stickle, P.E. Sobol, K.D. Bomben, J. Chastain, R.C. King Jr., Physical Electronics, Incorporation, eds., Handbook of X-ray photoelectron spectroscopy: a reference book of standard spectra for identification and interpretation of XPS data, Physical Electronics, Eden Prairie, Minn., 1995.
[32] B. Sefer, Environment related surface phenomena and their influence on properties of Ti-6Al-4V and Ti-6Al-2Sn-4Zr-2Mo : oxidation at elevated temperature and corrosion during chemical treatment, (2016).
[33] D. Mandrino, I. Paulin, S. Skapin, Scanning electron microscopy, X-ray diffraction and thermal analysis study of the TiH2 foaming agent, Mater Charact 72 (2012) 87–93, https://doi.org/10.1016/j.matchar.2012.07.005.
[34] R. Born, D. Scharnweber, S. Rößler, M. Stölzel, M. Thieme, C. Wolf, H. Worch, Surface analysis of titanium based biomaterials, Fresenius J Anal Chem 361 (1998) 697–700, https://doi.org/10.1007/s002160050997.
[35] A. Medvids, P. Onufrijevs, J. Kaupužs, R. Eglitis, J. Padgurskas, A. Zunda, H. Mimura, I. Skadins, S. Varnagiris, Anatase or rutile TiO2 nanolayer formation on Ti substrates by laser radiation: Mechanical, photocatalytic and antibacterial properties, Opt. Laser Technol. 138 (2021) 106898, https://doi.org/10.1016/j.optlastec.2020.106898.
[36] J.R. Ferraro, K. Nakamoto, C.W. Brown, Introductory Raman spectroscopy, 2nd ed,, Academic Press, Amsterdam; Boston, 2003.
[37] W.C. Saraswati, A. Anawati, I.N. Jujur, M.D. Gumelar, Effect of coloring by anodizing on the corrosion behavior of Ti-6Al-4V alloy, in: Tangerang Selatan, Indonesia, 2020: p. 020004. https://doi.org/10.1063/5.0001483.
[38] W.S. Tait, An introduction to electrochemical corrosion testing for practicing engineers and scientists, PairODocs Publ, Racine, Wisc, 1994.

[39] M. Ivašková, M. Lovíšek, K. Miková, Electrochemical Characteristics of Anodized Ti-6Al-4V Alloy, MSF 818 (2015) 149–152, https://doi.org/10.4028/www.scientific.net/MSF.818.149.
[40] M.B. Leban, T. Kosec, M. Finšgar, Corrosion characterization and ion release in SLM-manufactured and wrought Ti6Al4V alloy in an oral environment, Corros. Sci. 209 (2022) 110716, https://doi.org/10.1016/j.corsci.2022.110716.
[41] S. Hashimoto, A. Tanaka, Alteration of Ti 2p XPS spectrum for titanium oxide by low-energy Ar ion bombardment, Surf. Interface Anal. 34 (2002) 262–265, https://doi.org/10.1002/sia.1296.
[42] D. Prando, A. Brenna, M.V. Diamanti, S. Beretta, F. Bolzoni, M. Ormellese, M. Pedeferri, Corrosion of titanium: Part 2: Effects of surface treatments, Journal of Applied Biomaterials & Functional Materials 16 (2018) 3–13, https://doi.org/10.5301/jabfm.5000396.
[43] E.O. Ningrum, I. Khoiroh, H.I. Nastiti, R.A. Affan, A.D. Karisma, E. Agustiani, A. Surono, H. Suroto, S. Suprapto, L.S. Taji, S. Widiyanto, Surface Coating Effect on Corrosion Resistance of Titanium Alloy Bone Implants by Anodizing Method, Ijtech 14 (2023) 749, https://doi.org/10.14716/ijtech.v14i4.6146.
[44] L. Zhang, Y. Duan, R. Gao, J. Yang, K. Wei, D. Tang, T. Fu, The Effect of Potential on Surface Characteristic and Corrosion Resistance of Anodic Oxide Film Formed on Commercial Pure Titanium at the Potentiodynamic-Aging Mode, Materials 12 (2019) 370, https://doi.org/10.3390/ma12030370.
[45] N. Lin, Q. Liu, J. Zou, D. Li, S. Yuan, Z. Wang, B. Tang, Surface damage mitigation of Ti6Al4V alloy via thermal oxidation for oil and gas exploitation application: characterization of the microstructure and evaluation of the surface performance, RSC Adv. 7 (2017) 13517–13535, https://doi.org/10.1039/C6RA28421C.
[46] The Ellingham diagram, (n.d.). https://www.doitpoms.ac.uk/tlplib/ellingham_diagrams/ellingham.php (accessed June 1, 2023).
[47] M. Atapour, A. Pilchak, G.S. Frankel, J.C. Williams, M.H. Fathi, M. Shamanian, Corrosion Behavior of Ti-6Al-4V with Different Thermomechanical Treatments and Microstructures, 065004-065004–9, Corrosion 66 (2010), https://doi.org/10.5006/1.3452400.
[48] X. Zhou, D. Xu, S. Geng, Y. Fan, C. Yang, Q. Wang, F. Wang, Microstructural evolution and corrosion behavior of Ti–6Al–4V alloy fabricated by laser metal deposition for dental applications, J. Mater. Res. Technol. 14 (2021) 1459–1472, https://doi.org/10.1016/j.jmrt.2021.07.006.
[49] H.L. Du, P.K. Datta, D.B. Lewis, J.S. Burnell-Gray, Air oxidation behaviour of Ti6Al4V alloy between 650 and 850°, Corros. Sci. 36 (1994) 631–642, https://doi.org/10.1016/0010-938X(94)90069-8.
[50] Z.J. Liu, X. Zhong, J. Walton, G.E. Thompson, Anodic Film Growth of Titanium Oxide Using the 3-Electrode Electrochemical Technique: Effects of Oxygen Evolution and Morphological Characterizations, J. Electrochem. Soc. 163 (2015) E75, https://doi.org/10.1149/2.0181603jes.
[51] A. Yamagami, N. Nagaoka, K. Yoshihara, M. Nakamura, H. Shirai, T. Matsumoto, K. Suzuki, Y. Yoshida, Ultra-structural evaluation of an anodic oxidated titanium dental implant, Dent. Mater. J. 33 (2014) 828–834, https://doi.org/10.4012/dmj.2014-121.
[52] N. Khatun, P. Anita, D. Rajput, S.N. Bhattacharya, S. Jha, S. Biring, Sen, Anatase to rutile phase transition promoted by vanadium substitution in TiO2: A structural, vibrational and optoelectronic study, Ceram. Int. 43 (2017) 14128–14134, https://doi.org/10.1016/j.ceramint.2017.07.153.
[53] H. Guleryuz, H. Cimenoglu, Oxidation of Ti–6Al–4V alloy, J. Alloy. Compd. 472 (2009) 241–246, https://doi.org/10.1016/j.jallcom.2008.04.024.
[54] N. Vaché, Y. Cadoret, B. Dod, D. Monceau, Modeling the oxidation kinetics of titanium alloys: Review, method and application to Ti-64 and Ti-6242s alloys, Corros. Sci. 178 (2021) 109041, https://doi.org/10.1016/j.corsci.2020.109041.
[55] T. Qin, X. Lin, J. Yu, M. Wang, P. Guo, J. Li, Y. Zhang, J. Liu, S. Zhang, W. Huang, Performance of different microstructure on electrochemical behaviors of laser solid formed Ti–6Al–4V alloy in NaCl solution, Corros. Sci. 185 (2021) 109392, https://doi.org/10.1016/j.corsci.2021.109392.
[56] D.D. Macdonald, The Point Defect Model for the Passive State, J. Electrochem. Soc. 139 (1992) 3434–3449, https://doi.org/10.1149/1.2069096.
[57] M. Ask, J. Lausmaa, B. Kasemo, Preparation and surface spectroscopic characterization of oxide films on Ti6Al4V, Appl. Surf. Sci. 35 (1989) 283–301, https://doi.org/10.1016/0169-4332(89)90013-5.
[58] J. Lausmaa, Surface spectroscopic characterization of titanium implant materials, J. Electron Spectrosc. Relat. Phenom. 81 (1996) 343–361, https://doi.org/10.1016/0368-2048(95)02530-8.